The International Journal of Advanced Manufacturing Technology (2019) 100:1165–1182
https://doi.org/10.1007/s00170-018-1912-2

ORIGINAL ARTICLE

Viscoelastic medium modeling and surface roughness simulation of microholes finished by abrasive flow finishing process

Sachin Singh[1] · Deepu Kumar[1] · M. Ravi Sankar[1] · V. K. Jain[2]

Received: 14 March 2017 / Accepted: 14 March 2018 / Published online: 26 March 2018

Abstract
Surface roughness is one of the critical parameters that affect the component performance during its working life. To develop any process to its full potential, it is necessary to understand the physics of that process. Abrasive flow finishing (AFF) is one of the advanced finishing processes. In the current research work, an effort is made to understand physics and mechanism of surface roughness improvement during the AFF process. This research paper is divided into two sections. Firstly, the amount of finishing stresses and forces generated during the finishing of microholes fabricated on surgical stainless steel (316L) workpieces are computed by using the finite element method. Finishing stresses are generated in the viscoelastic medium. So, to compute finishing stresses, finite element analysis of the viscoelastic medium is carried out by incorporating its experimentally measured rheological properties. Finishing stresses are calculated along the circumferential direction of the microhole. Later, at the same workpiece surface location, simulated and experimentally measured surface roughness value are compared. Secondly, a new simulation model is proposed to predict the surface roughness on the microhole wall surface for various AFF input parameters. Maximum percentage change in surface roughness error of 8% is observed between simulated and experimental results after AFF process.

Keywords Finite element · Viscoelastic · Simulation · Surface roughness · Microholes

1 Introduction

Most of the advanced finishing processes use a flexible finishing tool that contains abrasive particles with random cutting edges. Also, these processes involve a large number of input variables. As a result, physics of an advanced finishing process due to their inherent random nature is not easy to understand. Modeling of the processes is one of the most effective and efficient method not only to understand the physics but also to develop a mechanism for controlling and optimizing the processes. Abrasive flow finishing (AFF) is one advanced finishing process which is very effective in finishing of macrocomponents to microcomponents having simple to complex geometries. However, AFF process with a vast number of input variables is very random in nature.

Figure 1a shows the model of AFF experimental setup used for finishing of microholes. At the start of AFF process, medium is filled in the lower medium cylinder. As the AFF experiment starts, the medium is extruded from the lower medium cylinder by the lower hydraulic cylinder piston, through the workpiece passage ways into the upper medium cylinder. Once the whole medium is discharged to the upper medium cylinder, the motion of the piston reverses. Microholes are fabricated by the electric discharge micromachining process (EDμM) on the surgical stainless steel (SS 316L) workpieces. The workpiece is then placed in between the upper and lower tooling (Fig. 1b). Complete assembly of tooling and workpiece is then kept securely between the upper and lower medium cylinder. To-fro motion of the medium through the workpiece passage ways causes the shearing of the workpiece surface roughness peaks by the abrasive particles mixed in the medium.

For understanding the mechanism of the AFF process, several researchers made efforts in three field's namely experimental, theoretical modeling, and numerical modeling. AFF

✉ M. Ravi Sankar
evmrs@iitg.ernet.in

[1] Department of Mechanical Engineering, Indian Institute of Technology Guwahati, Guwahati 781 039, India

[2] Department of Mechanical Engineering, Indian Institute of Technology Kanpur, Kanpur 208016, India

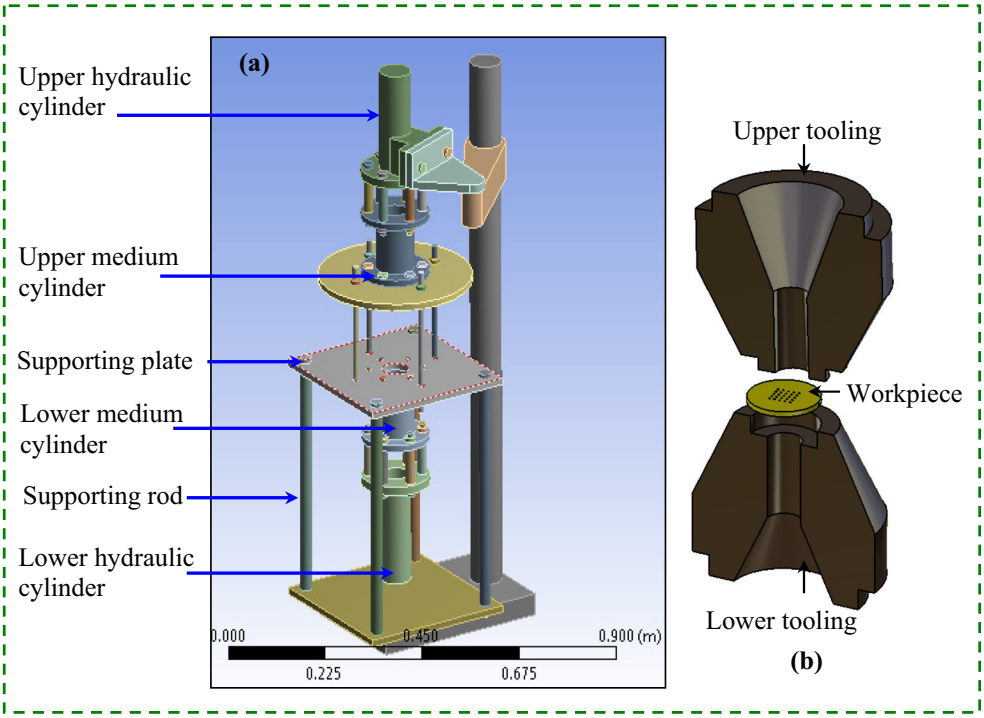

Fig. 1 Three-dimensional model of **a** abrasive flow finishing experimental setup and **b** tooling cross section with workpiece having microholes

experiments are conducted for finishing of workpieces with simple to complex geometries. Initially, researchers finished flat and cylindrical workpieces by the AFF process [1–3]. With the advancement of technology, researchers finished complex shape workpieces by the AFF process. Wu and Gao [4] finished bearing ring raceway by using AFF process, while Fu et al. [5] did finishing of blisk blades used in aero engines. To enhance the efficiency of the AFF process, Walia et al. [6] modified the AFF tooling by introducing a centrifugal force generating rod inside the cylindrical workpiece. Experimental studies carried out for understanding AFF process are greatly hampered by its random nature and involvement of many input variables. Also, extensive experiments cannot be performed due to the limitation of time, manpower, and resources. Hence, modeling is a more effective way for understanding physics of AFF process. Jain et al. [7] did 2D axisymmetric finite element (FE) analysis of the AFF process by considering the medium as Newtonian in nature. Later, Jain and Jain [8] replaced the Newtonian model with the Maxwell model to simulate the viscoelastic nature of the medium. Simulation of the surface roughness generated during the AFF process as a function of AFF input parameters is done by Jain and Jain [9]. Gorana et al. [10] developed theoretical model for calculating finishing forces and surface roughness obtained during the AFF process. Abrasive particle movement pattern during AFF process is predicted by the Fang et al. [11]. Wang et al. [12] used computation fluid dynamics (CFD) software to simulate medium flow and concluded that complex holes can be uniformly finished with the help of AFF process by using the tooling which is a replica of the workpiece to be finished. Wan et al. [13] used a non-Newtonian model that captures the medium flow. Dash and Maity [14] did the 2D and 3D simulation of the AFF process by considering the medium to behave as a Newtonian fluid having no slip at the workpiece surface. Chen and Cheng [15] used CFD software to study the motion of the AFF medium during the finishing of polygon holes by using helical passageways. Authors used the non-Newtonian power law to model the medium viscosity. Later, Wang et al. [16] to obtain the minimum surface roughness on the workpiece surface optimized the design of helical passageway. Singh et al. [17] did the theoretical modeling of the finishing forces generated during the AFF process. Extrusion pressure combined with rheology of the medium decides the amount of finishing forces generated in the medium during AFF experiments. Petri et al. [18] developed a neural network model that predicts surface roughness and dimensional changes in the workpiece during the AFF process. Mollah and Pratihar [19] modeled AFF process using radial basis function network.

Realizing the importance of the medium rheology, several researchers conducted experimental studies. Hull et al. [20] showed experimentally that AFF medium possesses time-dependent material properties. Davies and Fletcher [21] developed medium with various viscosities. Authors concluded that abrasive mesh size is the minor variable and temperature is the major variable affecting the viscosity of the medium. Fletcher and Fioravanti [22] developed a numerical model to predict thermal properties of the medium. Rheological (static and dynamic) properties of the medium and their role in deciding end surface roughness were studied by Sankar et al.

[23]. Kar et al. [24, 25] used five mediums of different base polymer. Mechanical as well as rheological study of the various mediums was done. Uhlmann et al. [26] tried to model the viscoelastic nature of the medium by Maxwell model and extended the same to generalized Maxwell model. Later, Uhlmann et al. [27] implemented the Maxwell model in the Ansys and carried out the simulation study of the AFF process.

As found out by the literature survey, theoretical model developed to predict the AFF process mechanism suffers from the disadvantage of too many variables to handle. So, the emphasis is given more on the numerical models. Viscoelastic medium is used during the AFF process, but most of the developed numerical models considered medium as Newtonian or non-Newtonian following power law. Very limited amount of work is reported in the literature related to the 3D modeling of the medium with viscoelastic properties. Existing models in literature provide the output as finishing stresses that are used as input parameter during simulation of the final surface roughness. So, the developed models are less realistic and result in considerable amount of error between the simulated and experimental value of surface roughness.

In the current research work, 3D FE analysis of the viscoelastic medium flow is carried out by incorporating the experimentally measured medium rheological properties as input parameters. Also, a novel simulation model to predict surface roughness during the AFF process as a function of input parameters (number of AFF cycles, extrusion pressure, and wt.% of abrasive particles) is proposed. In the literature, various authors experimentally and by using simulations predicted the surface roughness along the medium flow direction. So, simulation models are developed by incorporating 1D interaction between the abrasive particle and surface roughness peaks [7–10, 14]. However, no model is developed to predict the surface roughness in the perpendicular direction of the medium flow. In the present paper, experimental surface roughness is measured in the perpendicular direction to medium flow. Therefore, 2D interaction between the abrasive particle and surface roughness occurs, and the same is incorporated in developed roughness simulation model. Various efforts are made to develop a simulation model that predicts surface roughness nearer to experimental surface roughness (i.e., with minimal error).

2 Finite element simulation of the viscoelastic AFF medium

Finite element (FE) analysis to model the flow of viscoelastic medium during the AFF experiments is presented in the following section. FE analysis using ANSYS is divided into three steps:

2.1 Pre-processing

Pre-processing comprises of the following steps:

1. Geometry: All the AFF process setup components through which medium flows during the experiments are designed and assembled in ANSYS design modeler for carrying out FE analysis of the viscoelastic medium. Figure 2 shows the viscoelastic medium domain in which computational analysis is done during the processing step.
2. Meshing and setup: The meshed geometry of the viscoelastic domain is shown in Fig. 3a. Also, boundary conditions and material properties required during the solution step are assigned to the model. Model is divided into three sections namely inlet, outlet, and wall (Fig. 3b). Boundary conditions that are given to these sections are:

i. Inlet: At the inlet, the medium flows with the piston from the inlet to the outlet section. Thus, the conditions on inlet are chosen as

$$\textit{Inflow condition}, \quad F_n = F_0 \text{ (piston force) and } V_s = 0$$

ii. Outlet: At the outlet, normal force (piston force) is zero and medium does not flow tangentially [7]. Thus, the outlet boundary conditions are

$$\textit{Outflow condition}, \quad F_n = 0 \text{ and } V_s = 0.$$

iii. Wall: No slip boundary condition is assumed at the wall, i.e.,

$$V_s = V_n = 0$$

where F_n is normal force and V_s and V_n are tangential and normal velocities, respectively.

Medium rheological properties (static and dynamic) are measured with the help of Anton Paar MCR 101 rheometer (Fig. 4a). Experimentally measured material properties (Fig. 4b–d) are used as input during the FE analysis. The inclusion of the experimentally measured material properties makes the FE model more realistic. Thus, it helps in accurately evaluating the amount of finishing stresses generated in the medium from the FE analysis of the AFF process.

2.2 Processing

Viscoelastic model (Giesekus model) is used to simulate the behavior of the medium through contraction/expansion domain. Basic equations that govern the steady-state flow of incompressible viscoelastic medium by treating the medium as a continuum are laws of conservation of mass (continuity equation), conservation of momentum, and viscoelastic constitutive equation.

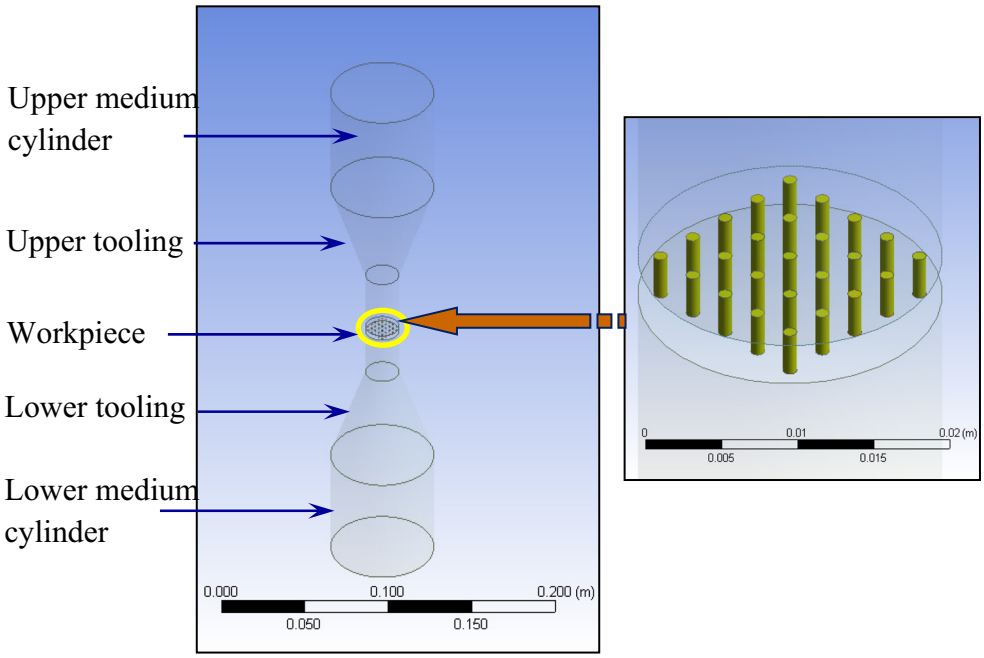

Fig. 2 Modeled domain of the viscoelastic medium of abrasive flow finishing process during finishing of microholes

2.2.1 Conservation of mass (continuity equation)

For the flow of steady-state incompressible medium flow, density is constant, i.e., independent of space and time. Therefore, the continuity equation reduces to

$$\nabla \bullet \widehat{U} = 0 \tag{1}$$

where $\hat{U}$ is the velocity vector.

2.2.2 Conservation of momentum

For steady, incompressible and isothermal flow conservation of momentum equation can be expressed as

$$\rho_m(\widehat{U} \bullet \nabla \widehat{U}) = \nabla \bullet T + f \tag{2}$$

where $T = -pI + \tau$ is the total extra stress tensor for incompressible medium, p = hydrostatic pressure, τ = extra stress tensor (component of total extra stress tensor), I unit tensor (identity tensor), f = internal forces expressed here as a force per unit volume (e.g., gravity), and ρ_m = density of the medium.

2.2.3 Viscoelastic constitutive equation (rheology model for abrasive medium)

To model the viscoelastic nature of the medium, one of the most realistic differential viscoelastic model, the so-called Giesekus model, is adopted. This model is commonly used for simulating the flow with shear thinning properties. Extra stress tensor is divided into two components namely viscoelastic component (σ_p) and purely viscous (Newtonian) component (σ_s) given as follows:

$$\tau = \sigma_p + \sigma_s \tag{3}$$

Giesekus model computes σ_p from the following equation:

$$\left(\mathrm{I} + \frac{\alpha\lambda}{\eta_1}\sigma_p\right).\sigma_p + \lambda\overset{\nabla}{\sigma_p} = 2\eta_1 D \tag{4}$$

where $\sigma_{\mathrm{p}}^{\nabla}$ is upper-convected derivative of viscoelastic extra stress which is defined as

$$\overset{\nabla}{\sigma_p} = \frac{D\sigma_p}{Dt} - \sigma_p \bullet \nabla\widehat{U} - (\nabla\widehat{U})^T \bullet \sigma_p \tag{5}$$

The Newtonian solvent contribution is given by

$$\sigma_s = 2\eta_2 D \tag{6}$$

where D is the rate of deformation tensor, I is the unit tensor (identity tensor), α is a material constant, λ is the relaxation time, η_1 is the viscosity factor for the viscoelastic component, and η_2 is the viscosity factor for the purely viscous component of the extra stress tensor.

2.3 Post-processing

During the post-processing step, radial finishing stresses generated on the surface of microhole during the AFF process are evaluated from medium flow FE model (Sects. 2.1 and 2.2). These stresses are later used to predict surface roughness. For modeling the finishing stresses firstly, governing equations

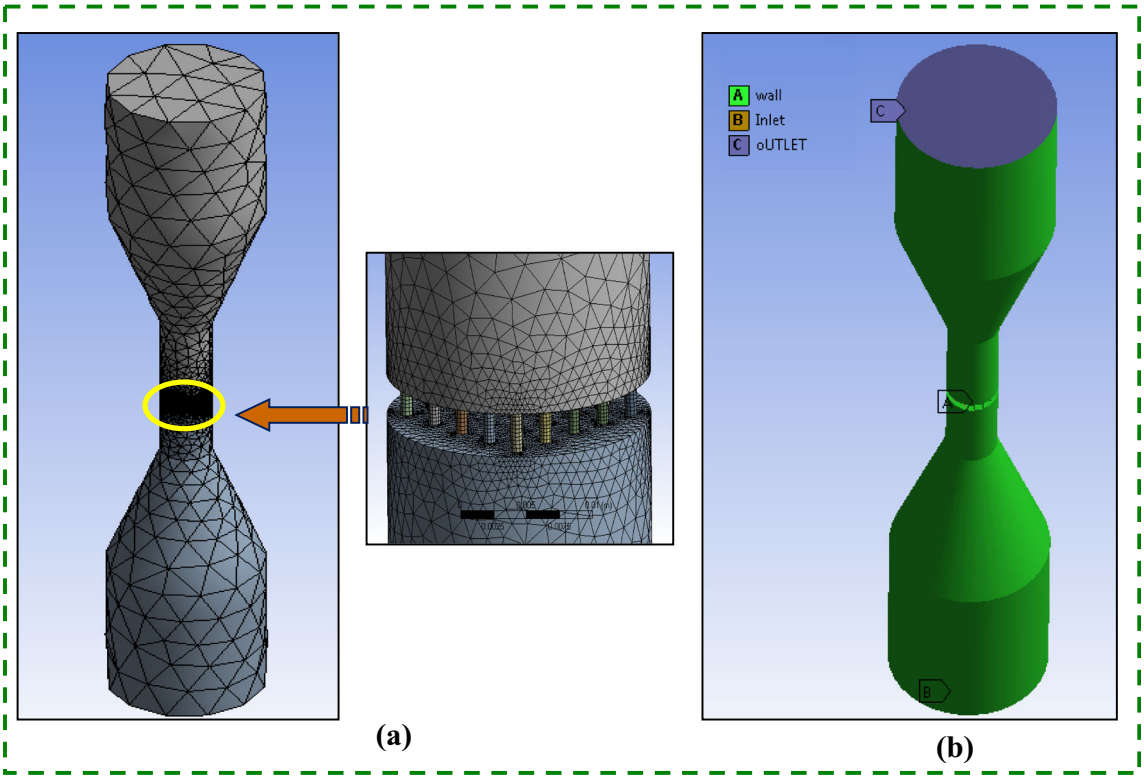

Fig. 3 Three-dimensional viscoelastic model showing **a** meshed geometry and **b** different boundaries

(conservation of mass, conservation of momentum, and viscoelastic constitutive equation) are solved by the Ansys Polyflow solver. In the post-processing step, radial finishing stresses are extracted from the nodes along the circumference of microhole FE model at two different locations (Fig. 5). Then, their average stress is taken to get the stresses at center surface of the microhole along the circumference.

3 Simulation of the surface roughness generated on microhole wall

The following assumptions are assumed during the simulation:

1. Abrasive particle size follows the normal distribution and is symmetric about the mean radius.
2. Shape of the abrasive particles is spherical.
3. Improvement in surface roughness occurs due to the microcutting of the surface roughness peaks.
4. Each abrasive particle consists of single cutting edge [7]. In the present paper, to simulate the surface roughness, during microcutting by abrasive particle, the single large cutting edge is split into small segments. Each small segment acts as a miniature cutting edge of the abrasive particle (Fig. 6). Thus, the abrasive particle is considered to possess multiple numbers of cutting edges. The X and Z coordinates of k^{th} cutting edge for j^{th} abrasive particle are given as x_{kaj} and z_{kaj}. Surface roughness profile is extracted from the workpiece surface by the 3D profilometer in the X and Z coordinates at an interval of 0.833 μm. Let x_{ir} and z_{ir} be the position coordinates defining the i^{th} roughness peak. Thus, by solving the equation of the circle (with center X^0_j, Z^0_j) for discrete values of x_{kaj} (i.e., at an interval of 0.833 μm), the corresponding z_{kaj} can be calculated. Therefore, the coordinates of cutting edge of the abrasive particles are calculated. Later, simulation of the cutting action is carried out. Detailed explanation of this mentioned phenomenon is presented in Sect. 3.2.

Average radial force (F_{Rj}) acting on j^{th} abrasive particle of diameter (D_{pj}) causes it to indent into a surface. This force is calculated by using the average radial stresses (σ_R) by the following formula [7]:

$$F_{Rj} = \sigma_R \frac{\pi D_{pj}^2}{4} \tag{7}$$

Brinell hardness number (BHN) takes care of the effect of workpiece material property on surface roughness during simulation of the AFF process. BHN is given by the following formula [7]:

$$\mathrm{BHN} = \frac{F_{Rj}}{{}^{\pi}/_{2}\, D_{pj}\left(D_{pj} - \sqrt{D_{pj}^2 - D_{idj}^2}\right)} \tag{8}$$

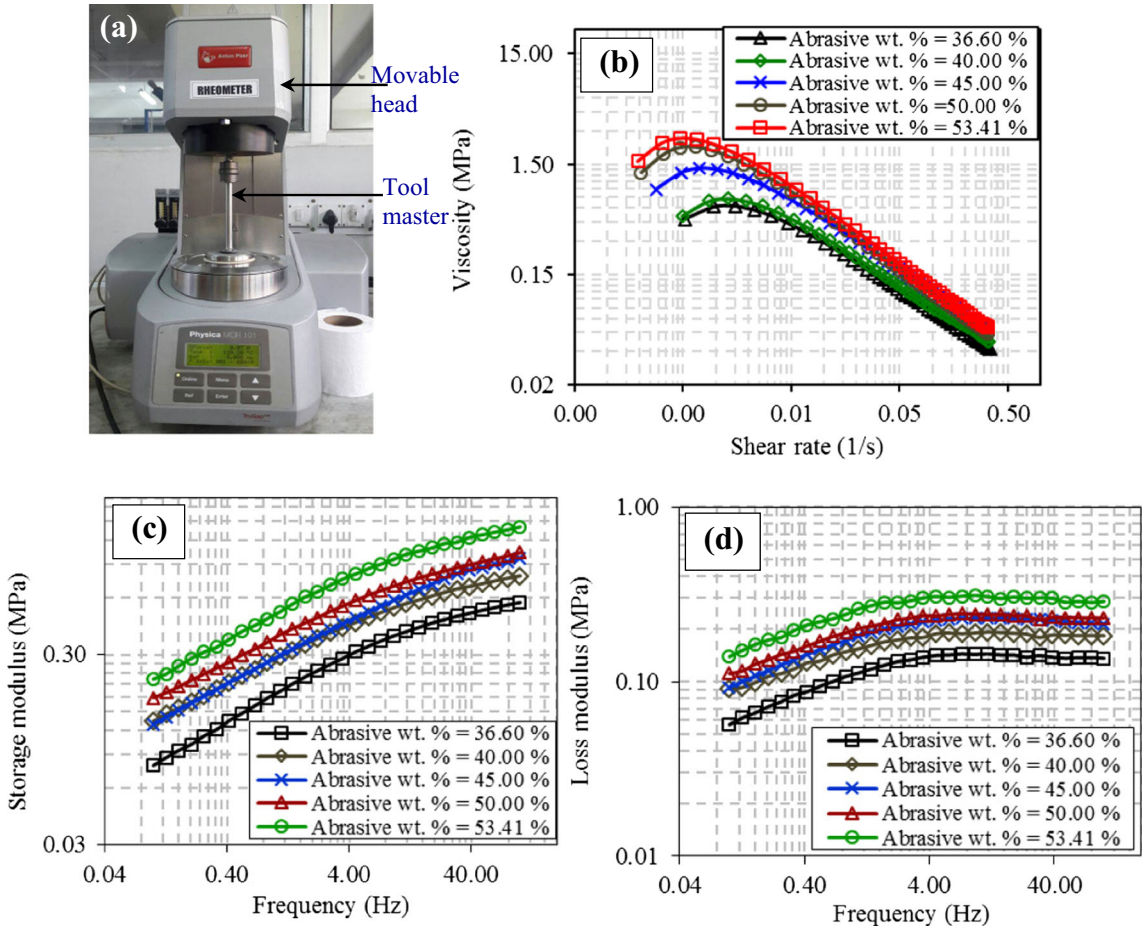

Fig. 4 **a** MCR-101 rheometer, rheological properties of the medium. **b** Viscosity variation with shear rate. **c** Storage modulus variation with frequency. **d** Loss modulus variation with frequency

BHN of the SS 316L workpiece is 209 BHN. Putting the value of F_{Rj} acting on the jth abrasive particle and D_{pj} diameter of j^{th} abrasive particle into Eq. 8, indentation diameter of the jth abrasive particle D_{idj} can be calculated. Maximum indentation depth (d_j) of the j^{th} abrasive particle into the workpiece surface (Fig. 7) is given as [7]

$$d_j = \frac{D_{pj}}{2} - \frac{1}{2}\sqrt{D_{pj}^2 - D_{idj}^2} \tag{9}$$

Procedure for generating the simulated surface roughness profile is divided into two sections:

1. Finding effective volume of the medium to be used during the AFF simulation.
2. Simulation of the cutting action of surface roughness peaks by abrasive particles.

3.1 Effective medium volume

The volume and dimensions of the fractionated medium (Fig. 8a) used in simulation are determined in the following way:

1. Total length of medium (AE = L_m) passed through 25 microholes in one stroke length (L_s) is given by

Volume of medium cylinder with R_m as radius = $\pi R_m^2 L_s$.

Cross-sectional area of one microhole with r_m as radius = πr_m^2.

Total cross-sectional area (A_s) of the medium passing through M number of microholes:

$$A_s = M \times \pi r_m^2$$

Therefore, the equivalent length of the medium (L_m) is given as

$$L_m = \frac{\pi R_m^2 L_s}{A_s} \tag{10}$$

2. Width (EH = L_a) of the medium is equal to the assessment length of the surface roughness profile which is measured from 3D surface roughness profilometer.
3. Height (AB = *Max. Z*+ *Max.* D_p) of the medium is taken as sum of maximum height of surface roughness peak "*Z*" in the assessment length of the surface roughness and

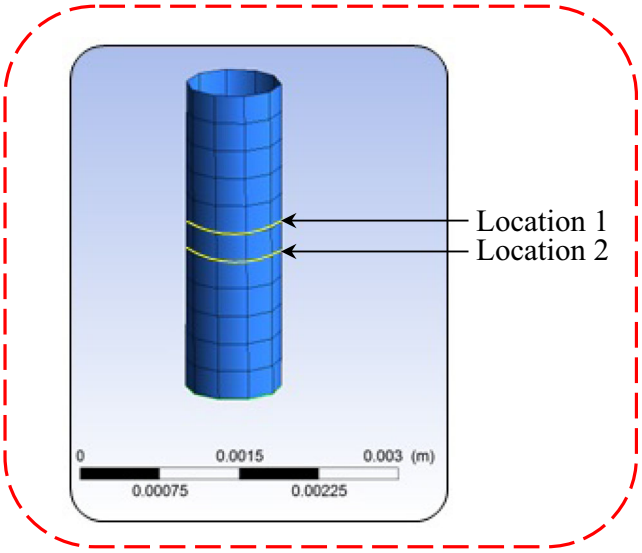

Fig. 5 Three-dimensional finite element model of microhole showing the location of stress evaluation

maximum diameter of abrasive particle that is generated by normal distribution. Above this height, abrasive particles are not going to take place in AFF cutting action. The abrasive particles which are below this height are going to remove the roughness peaks during AFF process (Fig. 8b).

Abrasive particles in the effective medium volume are generated as follows:

1. Overall mass of the abrasives in the effective medium volume is:

Volume of the medium (V_m) used in simulation of AFF process during one stroke can be given as

$$V_m = A_m \times L_m \tag{11}$$

where A_m is the cross-sectional area of the effective volume.

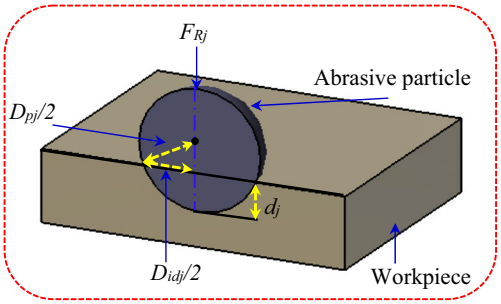

Fig. 7 Schematic diagram of the indentation of an abrasive particle on the workpiece surface [17]

Therefore, the overall mass of the abrasives (M_a) in the above medium volume is given by

$$M_a = \frac{\rho_m V_m C}{100} \tag{12}$$

where ρ_m is the density of the medium and C is the wt.% of the abrasive particles in the medium

Abrasive particles are generated with radius following the normal distribution and are symmetric about the mean radius (R_p) given as

$$R_p = \frac{R_a + R_b}{2} \tag{13}$$

The standard deviation (σ_d) of the abrasive particle radius is given as

$$\sigma_d = \frac{(R_b - R_a)}{6} \tag{14}$$

where R_b and R_a are the range for the radius of normally distributed abrasive particles having mean radius as R_p and standard deviation as σ_d.

Also, the relation between the radius of the abrasive particle (R_p) and mesh size (M_p) is given as [9]

$$R_p\,(\text{mm}) = \frac{7.62}{M_p} \tag{15}$$

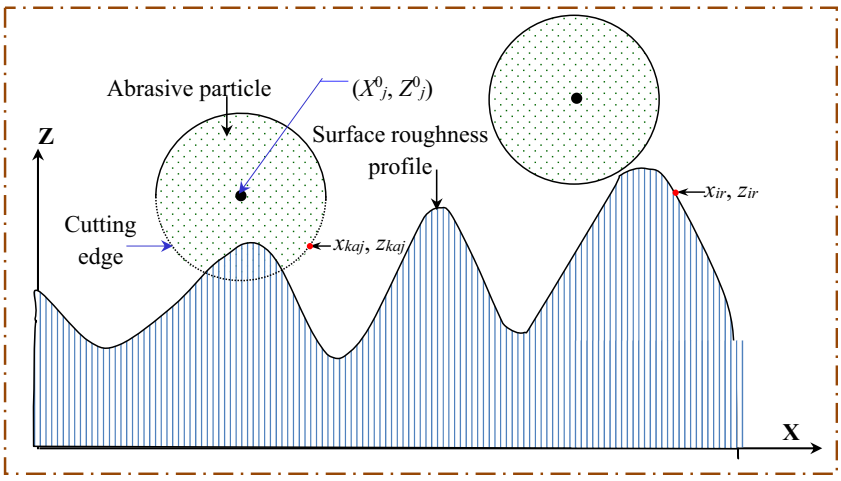

Fig. 6 Schematic showing the interaction between abrasive particle and workpiece surface roughness

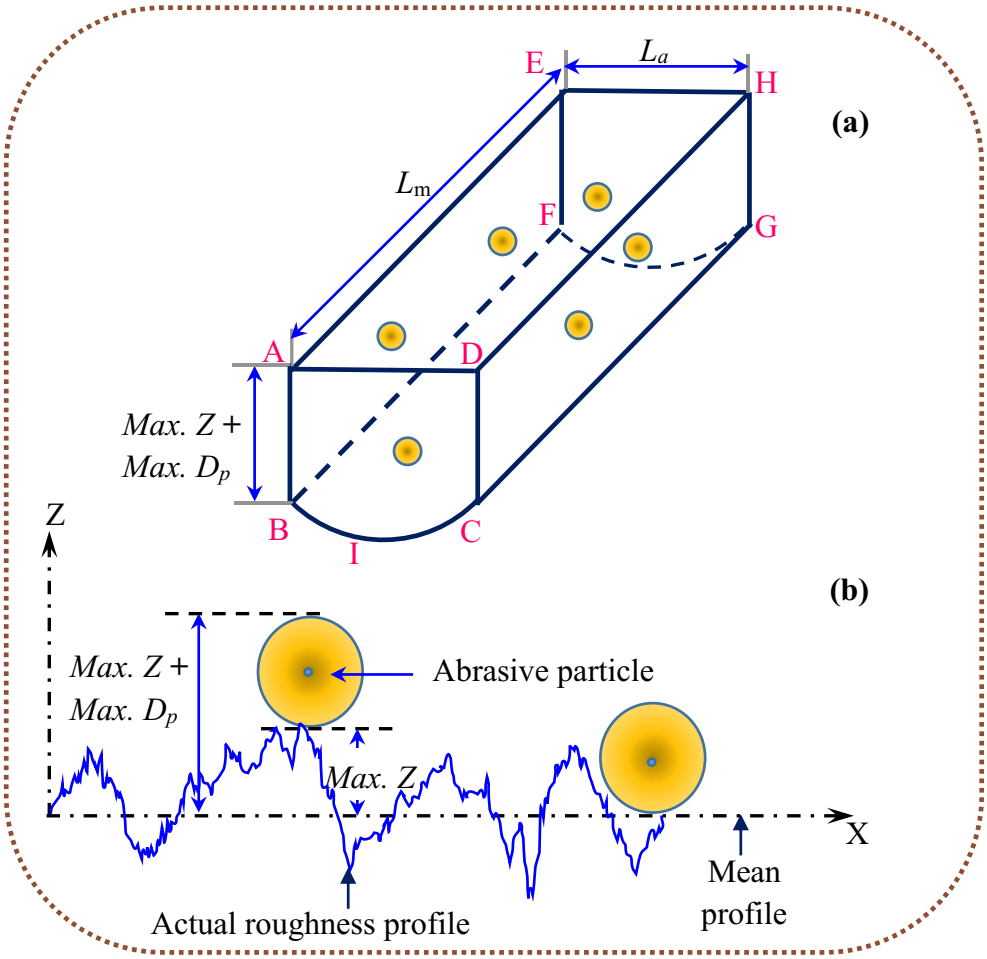

Fig. 8 **a** Schematic view showing the dimensions of medium slug containing abrasive particles used during the surface roughness simulation. **b** Two-dimensional schematic of surface roughness profile

2. Abrasive particles (N_a) in the medium volume are generated until the sum of individual abrasive particle is equal to the total mass of abrasive particles, i.e.,

$$\frac{4}{3}\Pi\rho_a \sum_{j=1}^{N_a} R_{Pj}^3 = M_a \tag{16}$$

where ρ_a is the density of the abrasive particles and R_{pj} is the radius of the j^{th} abrasive particle.

3. Condition for avoiding overlapping of the abrasives

During AFF process simulation, abrasive particles are randomly generated which may sometimes result in overlapping of some abrasive particles. Hence, to overcome this, $(j-1)^{th}$ and j^{th} abrasive particles are subjected to a condition that the centers of two generated abrasive particles should be apart by a distance which is greater or equal to the sum of their radii, i.e.,

$$\sqrt{\left(X_{j-1}^0 - X_j^0\right)^2 + \left(Y_{j-1}^0 - Y_j^0\right)^2 + \left(Z_{j-1}^0 - Z_j^0\right)^2} \geq \left\{(R_P)_{j-1} + (R_P)_j\right\} \tag{17}$$

where $(X^0_{j-1}Y^0_{j-1}, Z^0_{j-1})$ and (X^0_j, Y^0_j, Z^0_j) are center coordinates of the $(j-1)$th and jth abrasive particles, respectively.

3.2 Simulating of the cutting action of surface roughness peaks during abrasive flow finishing of microholes

Real initial surface roughness profile is incorporated during simulation of the cutting action of roughness peaks. This inclusion makes the surface roughness simulation model more realistic. From the workpiece, a small strip is taken out containing microhole with the help of wire electric discharge machining (WEDM) process (Fig. 9a, b). Using non-contact type profilometer, 3D surface topography (area of 130 μm × 130 μm) of microhole-finished region is obtained. Two dimensional surface roughness profile data in the circumferential direction (along the line drawn in the center half of the image) from the 3D image is extracted in the form of X and Z coordinates (Fig. 9c).

"X" is the position of the roughness peak along the assessment length of the workpiece, and "Z" is its corresponding height. Figure 9d shows initial surface roughness profile data over an assessment length (L_a) of 130 μm which is taken from 3D surface roughness profilometer.

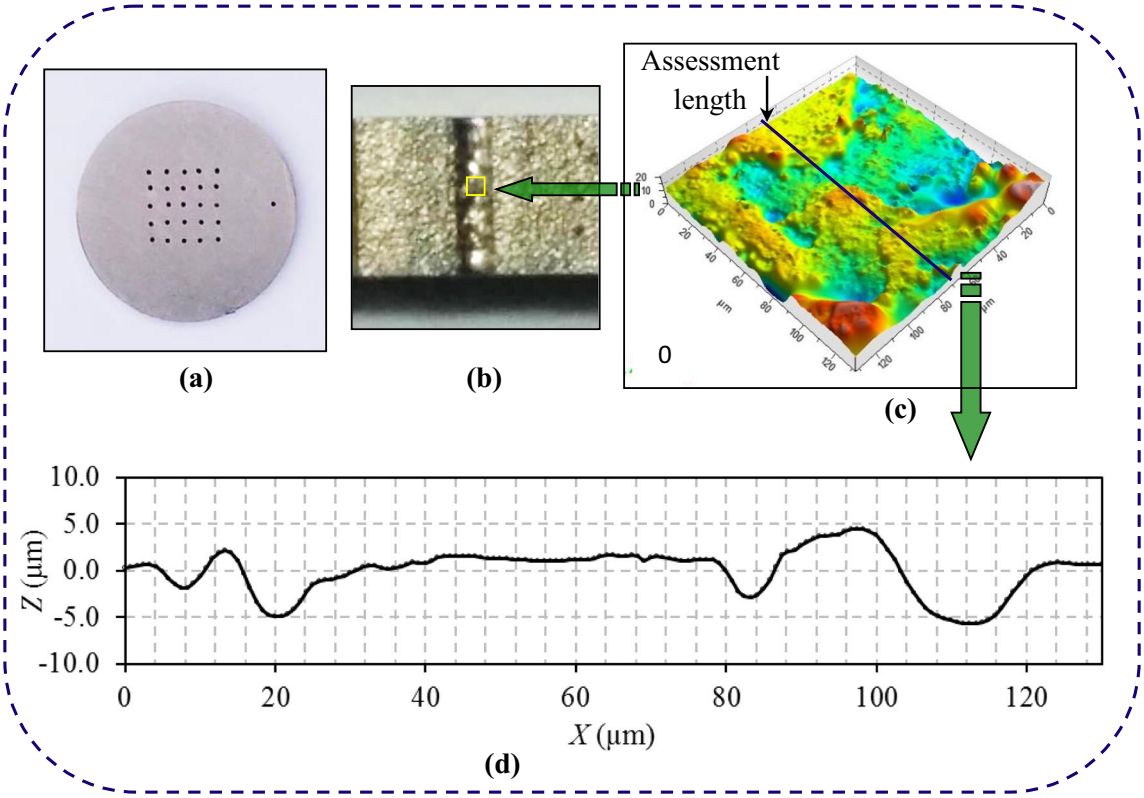

Fig. 9 **a** Workpiece. **b** Cut surface of the microhole. **c** 3D surface topography of the workpiece. **d** Two-dimensional roughness profile of the workpiece surface (R_a = 1.38 μm)

Surface roughness profile is measured in a direction perpendicular to the medium flow. Thus, there is a 2D (X, Z) interaction of the abrasive particle with the surface roughness peaks. Surface roughness profile data taken by the profilometer is for a length of 130 μm. X and Z coordinates of the roughness profile are generated at an interval of 0.833 μm (Fig. 9d). Therefore, a total of 156 roughness points define the roughness profile in the assessment length. Let x_{ir} be the X coordinate of the ith roughness peak having z_{ir} as corresponding height in the Z coordinate. Also, in the whole assessment length, let z_m be the maximum height of the roughness peak for a particular AFF stroke.

Cutting action is performed in the following steps:

1. Finding the maximum number of cutting edges of an abrasive particle that can take part in cutting action during an AFF stroke

Maximum roughness height that can be overlapped by the abrasive particle during an AFF stroke is z_m. Thus, z_m is the maximum height of the cutting edge of the abrasive particle that can take part in the cutting action of the roughness peak. The X coordinate of i^{th} cutting edge of the j^{th} abrasive particle (x_{iaj}) corresponding to z_m can be calculated as

$$\left(x_{iaj}-X_j^0\right)^2+\left(z_m-Z_j^0\right)^2=R_{pj}{}^2 \tag{18}$$

Therefore, the number of cutting edges N_{maxj} (N_{maxj}, if comes in decimal, then next whole number) on the left side of the diameter of the j^{th} abrasive particle that can take part in the cutting action of the roughness peak is

$$N_{maxj}=\frac{x_{iaj}}{0.833} \tag{19}$$

Thus, the maximum numbers of cutting edges of the jth abrasive particle that can take part in the cutting action of roughness peak (N_{tmaxj}) are

$$N_{tmaxj}=2N_{maxj}(both\quad sides\quad of\quad the\quad diameter)+1\,(center\quad point) \tag{20}$$

2. Shifting of the abrasive particle

X coordinate of the j^{th} abrasive particle center is shifted to their nearest X coordinate at which surface roughness profile is defined. As shown in Fig. 10, center of the abrasive particle is updated as

$$newX_j{}^0=x_{nr} \tag{21}$$

Now, for the same X coordinate (x_{lr}), there is j^{th} abrasive particle's k^{th} edge having Z coordinate (z_{kaj}) and a roughness peak having Z coordinate (z_{lr}), respectively (Fig. 10).

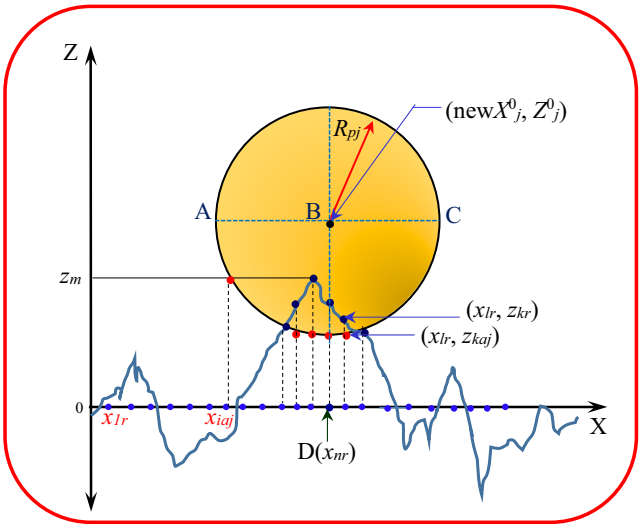

Fig. 10 Schematic view of 2D interaction of an abrasive particle with the surface roughness profile during simulation of AFF process

3. Determination of the Z coordinate of the abrasive particle cutting edges

N_{tmaxj} number of cutting edges of j^{th} abrasive particle are generated whose Z coordinates are given by the following equation:

$$\left(x_{nr}-newX_j^0\right)^2+\left(z_{naj}-Z_j^0\right)^2=R_{pj}{}^2 \tag{22}$$

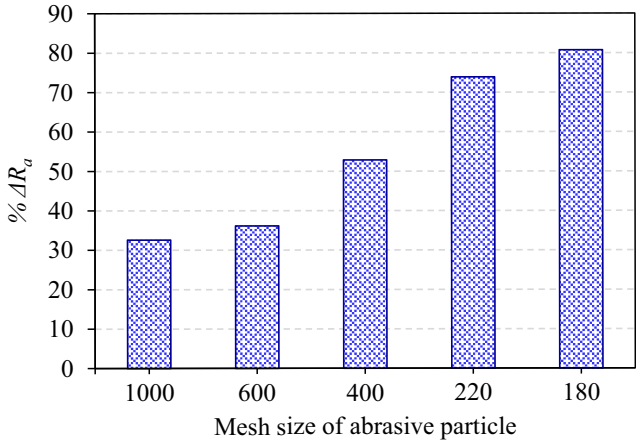

Fig. 12 Variation of percentage change in surface roughness with mesh size of the abrasive particles (8 cycles, 4 MPa, 35 wt.% abrasive particles)

i. Z coordinates of the j^{th} abrasive particle cutting edges in the left side of the abrasive particle (ABD) are given when x_{nr} is given as

$$x_{nr}=newX_j^0-n\times 0.833 \quad \text{for } n=1 \text{ to } N_{maxj} \tag{23}$$

ii. Z coordinates of the j^{th} abrasive particle cutting edges in the right side of the abrasive particle (CBD) are given when x_{nr} is given as

$$x_{nr}=newX_j^0+n\times 0.833 \quad \text{for } n=1 \text{ to } N_{maxj} \tag{24}$$

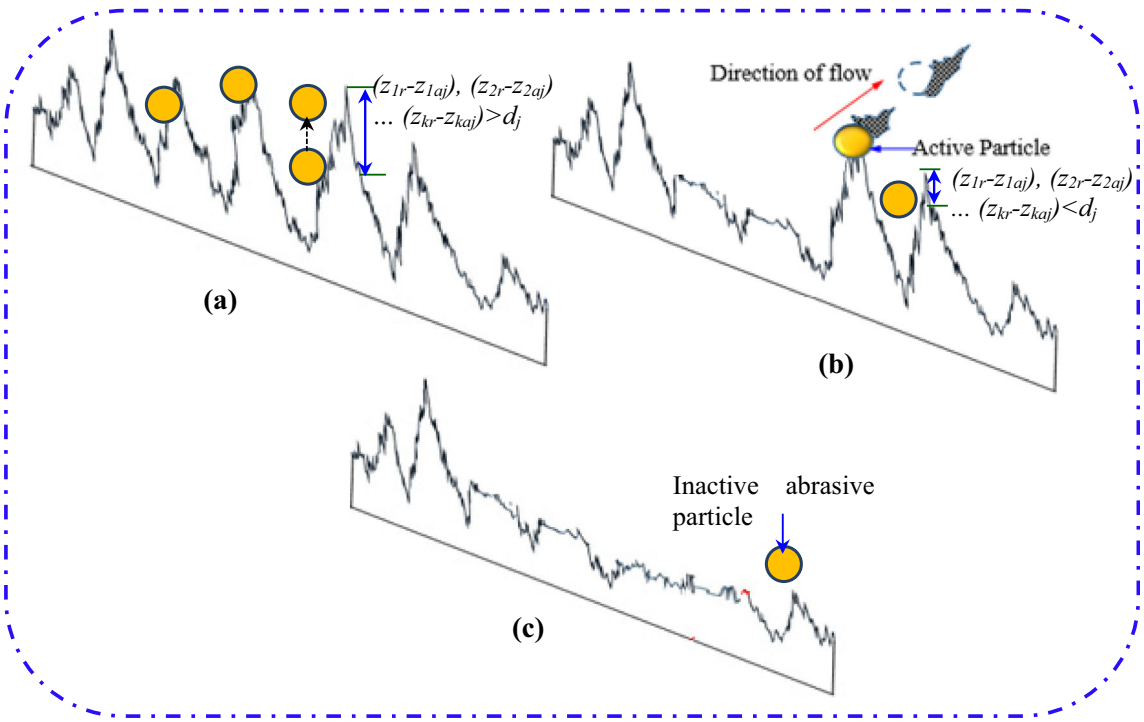

Fig. 11 Schematic view of simulation of AFF cutting action for different cases. **a** Indentation depth of abrasive particle cutting edges is greater than maximum indentation depth. **b** Indentation depth of abrasive particle cutting edges is less than maximum indentation depth. **c** Abrasive particle not indenting into the workpiece surface

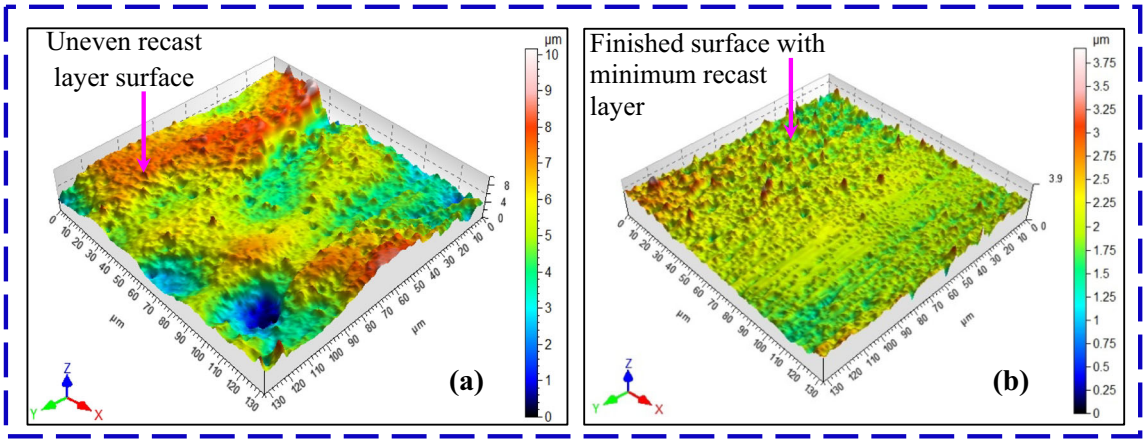

Fig. 13 Surface topography images of the workpiece surface at various mesh sizes. **a** 1000 ($R_a = 0.98$ μm). **b** 180 ($R_a = 0.26$ μm) (8 cycles, 4 MPa, 35 wt.% of the abrasive particles)

iii. Z coordinates of the central cutting edge (D) is given when x_{nr} is given as

$$x_{nr} = new X_j^0 \tag{25}$$

4. Cutting of the surface roughness peaks

For the j^{th} abrasive particle, comparison is made between the Z coordinate of abrasive particle cutting edges (z_{1aj}, z_{2aj}……z_{kaj}) and corresponding Z coordinate of the roughness peak (z_{1r}, z_{2r}……z_{kr}) for the same X coordinate. Depending on their relative positions, cutting is done.

As the abrasive particles are randomly generated in the medium volume, the following three cases arise for the cutting of the surface roughness peaks during the AFF process:

i. Difference between some of the Z coordinates of the roughness peak and corresponding Z coordinates of j^{th} abrasive particle cutting edges is more than its maximum depth of the indentation (d_j) (Fig. 11a), i.e.,

$$\begin{aligned}&\left(z_{1r}-z_{1aj}\right), \left(z_{2r}-z_{2aj}\right), \left(z_{3r}-z_{3aj}\right)\ldots\ldots\ldots\left(z_{kr}-z_{kaj}\right)\\ &> d_j; k = 1 \text{ to} N_{tmaxj}\end{aligned} \tag{26}$$

During the experimentation, abrasive particles can remove the roughness peaks from the workpiece surface in the form of microchips/nanochips only if they indent into the workpiece surface upto d_j. However, if the abrasive particles indent beyond d_j, then the force needed for removing the material is more than the applied finishing force by the abrasive particles. As a result, abrasive particles only make indentation marks on the workpiece surface. Later, indented abrasive particle adjusts itself in upcoming AFF cycles until it reaches the depth d_j after that it moves in the axial direction [28]. The same phenomenon is included during simulation. If abrasive particle cutting edges indent more than d_j, then to reach d_j, it adjusts in the following way:

a. The maximum positive difference between the Z coordinates of jth abrasive particle cutting edge and the corresponding Z coordinates of the roughness peak is found out, i.e.,

$$\begin{aligned}&Max\left[\left(z_{1r}-z_{1aj}\right), \left(z_{2r}-z_{2aj}\right), \left(z_{3r}-z_{3aj}\right)\ldots\ldots\ldots, \left(z_{kr}-z_{kaj}\right)\right]\\ &= M_j;\ \ k = 1 \text{ to} N_{tmaxj}\end{aligned} \tag{27}$$

b. The abrasive particle is shifted upwards with respect to the workpiece surface. This is done by updating the Z coordinate of abrasive particle cutting edges in the following way:

$$\begin{bmatrix} z_{u1aj} = z_{1aj} + \left(M_j - d_j\right) \\ z_{u2aj} = z_{2aj} + \left(M_j - d_j\right) \\ . \\ . \\ . \\ z_{ukaj} = z_{kaj} + \left(M_j - d_j\right) \end{bmatrix} k = 1 \, to N_{tmaxj} \tag{28}$$

Table 1 Abrasive flow finishing input parameters their coded and absolute values

S. no.	AFF input parameter	Unit	Levels				
			− 1.682	− 1.000	0.000	1.000	1.682
1.	Extrusion pressure (P)	MPa	~3.20	3.50	4.00	4.50	~4.90
2.	No. of AFF cycles (N)	–	~4.50	6.00	8.00	10.00	~11.50
3.	Wt.% of abrasives (W)	%	36.60	40.00	45.00	50.00	53.40

Table 2 Values of various parameters used during simulation

Hardness of the workpiece material	209 BHN
Radius of microholes (mm)	0.425
Radius of medium cylinder (mm)	30
Stroke length (mm)	68
Maximum and minimum mesh size of the SiC abrasive particle (μm)	170–190
Density of abrasive particles (kg/m^3)	3220

where z_{u1aj}, z_{u2aj}.....z_{ukaj} are the updated Z coordinates of the j^{th} abrasive particle.

Now, the abrasive particle is at the maximum depth of indentation. So, to simulate the cutting action, the Z coordinates of the roughness peak that are below the Z coordinates of the j^{th} abrasive particles are updated as

$$\begin{bmatrix} z_{1r} = z_{u1aj} \\ z_{2r} = z_{u2aj} \\ . \\ . \\ . \\ z_{kr} = z_{ukaj} \end{bmatrix} k = 1 \text{ to} N_{tmaxj} \tag{29}$$

ii. Difference between some of the Z coordinates of the roughness peak and corresponding Z coordinates of the j^{th} abrasive particle cutting edges is less than d_j (Fig. 11b), i.e.,

$$\left(z_{1r}-z_{1aj}\right), \left(z_{2r}-z_{2aj}\right), \left(z_{3r}-z_{3aj}\right).....\left(z_{kr}-z_{kaj}\right) < d_j; k = 1 \text{ to} N_{tmaxj} \tag{30}$$

Then, the cutting action of the roughness peak is performed by updating the Z coordinate of the roughness peaks as

$$\begin{bmatrix} z_{1r} = z_{1aj} \\ z_{2r} = z_{2aj} \\ . \\ . \\ . \\ z_{kr} = z_{kaj} \end{bmatrix} k = 1 \text{ to} N_{tmaxj} \tag{31}$$

iii. When all the generated Z coordinates of the abrasive particle cutting edges lie above the corresponding Z coordinate of the roughness (Fig. 11c), i.e.,

$$\left(z_{1r}-z_{1aj}\right), \left(z_{2r}-z_{2aj}\right), \left(z_{3r}-z_{3aj}\right).....\left(z_{kr}-z_{kaj}\right) < 0; k = 1 \text{ to} N_{tmaxj} \tag{32}$$

In that circumstance, the abrasive particle becomes an inactive particle which does not take part in cutting action of surface roughness peak. In such cases, Z coordinate of the roughness peaks remains the same. Completion of one AFF stroke is marked by passing all the generated abrasive particles (N_a) over the roughness peak. After the completion of one AFF stroke, surface roughness value (R_{as}) is calculated and the mean line is shifted as

$$R_{as} = \frac{1}{L_a}\int_0^{L_a} |Z(x)|\, dx \tag{33}$$

Before the commencement of the next AFF stroke, the number of cutting edges for j^{th} abrasive particle (N_{tmaxj}) is calculated based on the updated value of z_m. All the above-outlined steps are repeated till the required number of AFF cycles is completed. During finishing processes, a critical surface roughness (R_c) exists due to the indentation of the abrasive particles on the workpiece surface. Beyond R_c, abrasive particle is not able to remove the material from the workpiece surface. Therefore, there is no improvement in the surface roughness beyond R_c and is given as [7]

$$R_c = \frac{D_{pj}}{2} - \frac{1}{2}\sqrt{D_{pj}^2 - D_{idj}^2} \tag{34}$$

4 Experimentation

Microholes in an array of 5 × 5 having diameter 850 μm are fabricated on the surgical stainless steel (316L) workpiece with the help of EDμM process. Surface roughness before and after the AFF process is measured with the help of 3D surface profilometer (Make: Taylor Hobson). Initial surface roughness on the microhole wall varies in the range of 1.40 ± 0.10 μm.

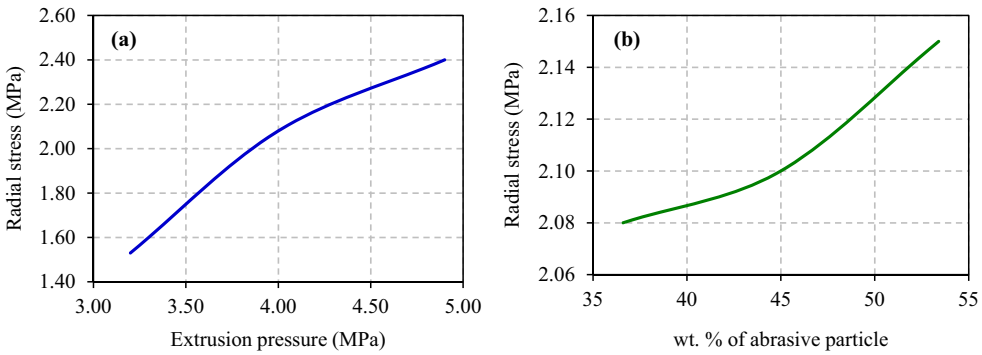

Fig. 14 Variation of radial stresses generated in the medium with respect to **a** extrusion pressure and **b** wt.% of abrasive particles in the medium

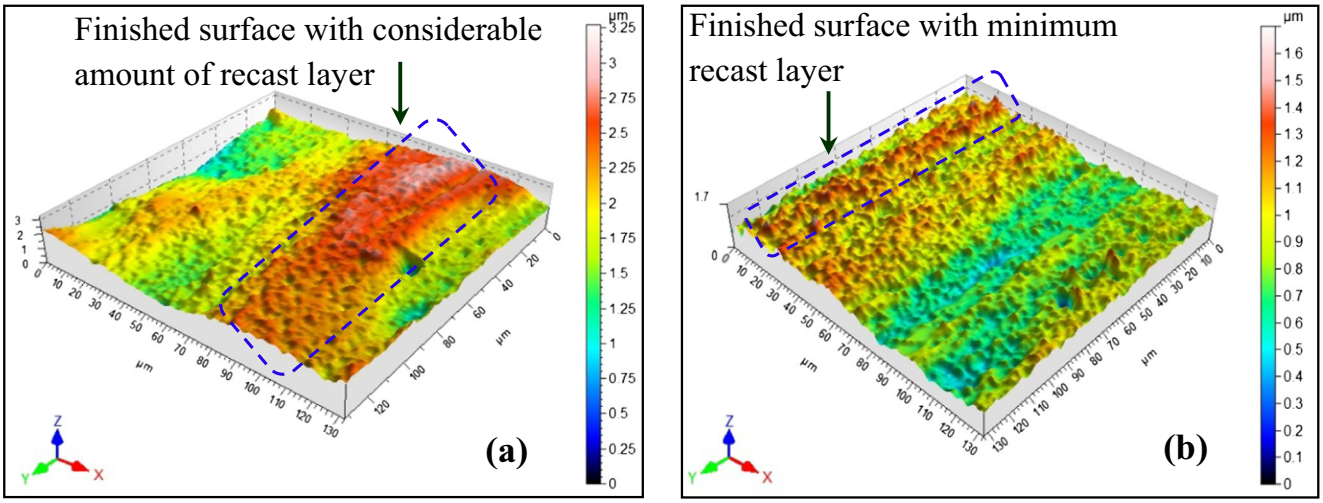

Fig. 15 Surface topography images of the workpiece surface after finishing at various extrusion pressure. **a** 3.20 MPa (R_a = 0.31 µm). **b** 4.90 MPa (R_a = 0.15 µm) (8 cycles, # 180, 45 wt.% of the abrasive particles)

It is found from the experimental observations that the larger the size of the abrasive particle, the more effectively it shears the surface roughness peak. Figure 12 shows the effect of abrasive particle mesh size (#) on % ΔR_a. Workpiece surface becomes uniform with improved surface roughness after finishing them with smaller mesh size abrasive particles (Fig. 13a, b). AFF experiments with the medium having # 180 mesh size abrasive particles give the highest improvement in surface roughness. Therefore, medium with various wt.% of # 180 mesh size abrasive particles is used during the parametric study of the AFF process during finishing of the microholes.

Effect of three important AFF process input parameters namely extrusion pressure (P), number of AFF cycles (N), and wt.% of the abrasive particles in the medium (W) is studied on the percentage change in surface roughness, % ΔR_a (= (initial roughness − final roughness) × 100 / initial roughness). Experiments are designed by using the central composite rotatable design (CCRD) method. Based on the number of input variables and their different levels, CCRD method gives a particular set of experiments. In current paper, two-level full factorial design is used which gives 2^j factorial runs, 2j axial runs, and 6 central runs, where "j" is the number of input parameters (in the current paper, j = 3, factorial runs = 8, axial runs = 6). Thus, CCRD helps in studying individual and interaction effects of input parameters on output responses with minimum experiments compared to full factorial design. The output responses obtained after performing experiments are analyzed using response surface methodology which gives regression equations relating each output response as a function of input parameters. Table 1 shows the values of AFF input parameters used while designing the CCRD set of experiments. To maintain the accuracy in the regression equation, model terms up to second order are considered. The regression equation for experimental value of percentage

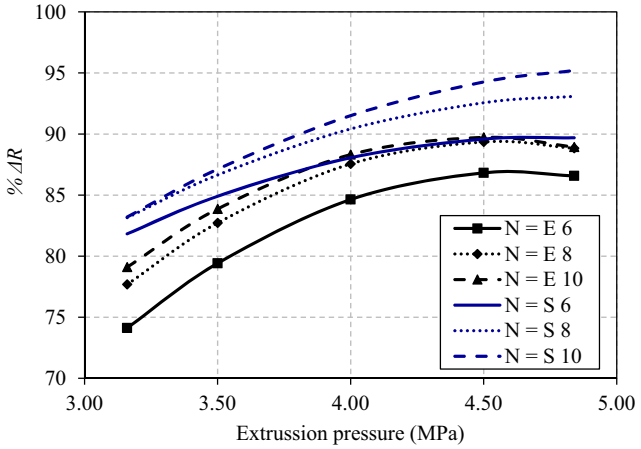

Fig. 16 Effect of extrusion pressure for different number of AFF cycles on percentage change in surface roughness (% ΔR_a, % ΔR_{as}) (wt.% of abrasives = 45%, # 180) (E stands for experiments, and S stands for the simulation)

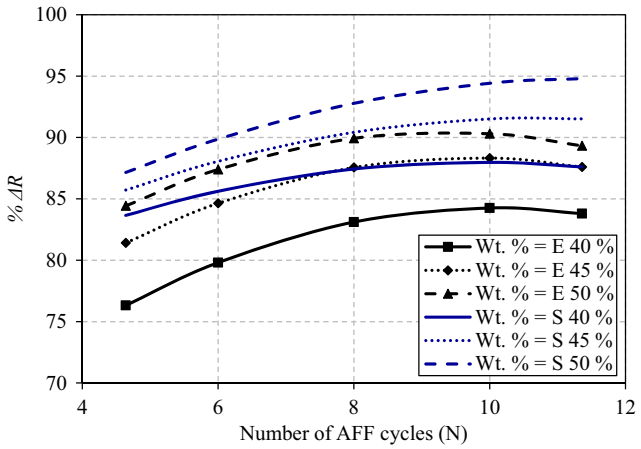

Fig. 17 Effect of number of AFF cycles for different wt.% of abrasive particles on percentage change in surface roughness (% ΔR_a, % ΔR_{as}) (extrusion pressure = 4 MPa, # 180) (E stands for experiments, and S stands for the simulation)

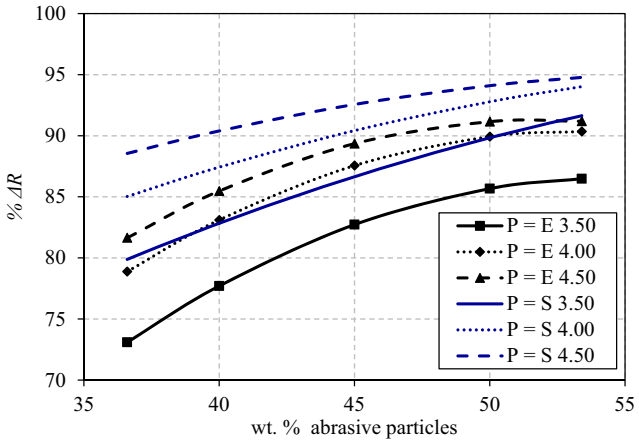

Fig. 18 Effect of wt.% of abrasive particles for different extrusion pressure on percentage change in surface roughness (% ΔR_a, % ΔR_{as}) (number of AFF cycles = 8, # 180) (E stands for experiments, and S stands for the simulation)

change in surface roughness, % ΔR_a in terms of AFF input parameter, is given as

$$\%\Delta R_a = -243.58 + 68.75P + 8.54N + 5.65W - 0.39PN - 0.23PW - 3.85 \times 10^{-2}NW - 6.09P^2 - 0.27N^2 - 0.04W^2 \quad (35)$$

Simulated results of percentage change in surface roughness, % ΔR_{as}, are also fitted by using regression model whose equation is given as

$$\%\Delta R_{as} = -72.10 + 41.90P - 1.52N + 2.55W - 0.61PN - 0.40PW - 5.50 \times 10^{-2}NW - 3.26P^2 - 0.16N^2 - 0.01W^2 \quad (36)$$

5 Results and discussion

The present section is divided into two parts. Firstly, the finishing stresses generated in the medium as found out from the FE analysis of the viscoelastic medium during the finishing of the microholes are presented. Later, using these evaluated stress values, simulation of the surface roughness generated on the microholes wall after the AFF process is presented. Simulated results are compared with the experimental results, and they are found in good agreement. Values of the various input parameters that are used during the simulation are given in Table 2.

5.1 Finishing stresses

During the AFF experiments, it is the finishing stresses generated in the medium (currently, it is extrusion pressure) which is responsible for cutting the surface roughness peaks on the workpiece surface by the action of abrasive particles. Finishing stresses generated in the medium are transferred to the abrasive particles by the medium. Radial stresses that are generated in the medium help in indentation of the abrasive particles in the workpiece surface. As the amount of extrusion pressure increases, the magnitude of radial stresses acting on the abrasive particles (Fig. 14a) also increases. Also, increase in wt.% of the abrasive particles increases medium viscosity. High viscous medium resists the inward movement of the abrasive particles in the medium and provides a firm support to the abrasive particles during their interaction with the workpiece surface. Thus, radial stresses generated in the medium are efficiently transferred to the workpiece surface by the abrasive particles during the cutting of roughness peaks. Thus, radial stresses increase with the increase in wt.% of the abrasive particles in the medium (Fig. 14b).

5.2 Surface roughness

5.2.1 Effect of extrusion pressure

Extrusion pressure is one of the important AFF input parameters that decides the amount of end surface roughness

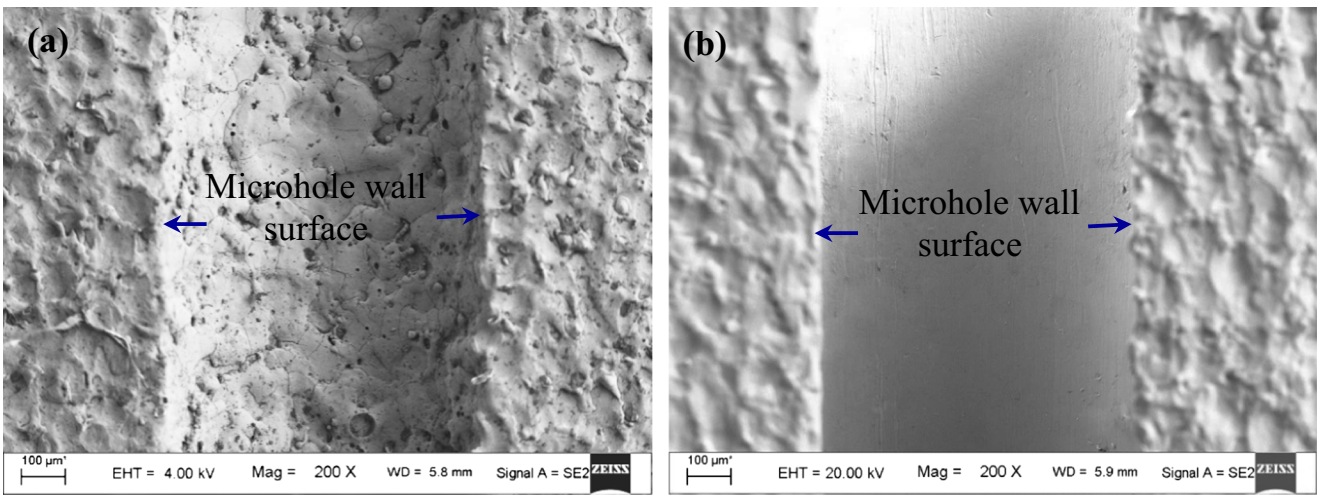

Fig. 19 Surface morphology images of the microhole finished by AFF process **a** before finishing and **b** after finishing (8 cycles, # 180, 4 MPa, 53.40 wt.% abrasives particles)

achieved on the workpiece surface after AFF process. As the extrusion pressure increases, more is the amount of radial stresses generated in the medium (Fig. 14a). These radial stresses help the abrasive particles in the effective and efficient cutting of surface roughness peaks from microhole wall. As a result, surface roughness improves with the increase in extrusion pressure (Fig. 15a, b). Microholes fabricated by the EDμM process leads to the formation of recast layer which is harder than the parent material on their surfaces. On the other hand, parent material hardness is incorporated during the simulation of the surface roughness. As a result, the resistance provided by the workpiece surface to the abrasive particles during cutting of the roughness peaks is higher during experiments compared to the simulation. Therefore, the magnitude of % ΔR_{as} is more as compared to % ΔR_a. Also, during the simulation, it is assumed that the amount of finishing stresses generated in the medium is transferred to the abrasive particle in the same amount which is not the case while performing AFF experiments. This further increases the magnitude of % ΔR_{as} as compared to % ΔR_a (Fig. 16).

5.2.2 Effect of number of AFF cycles

Surface roughness improvement during the AFF process takes place due to the repeated indentation of the abrasive particles on the surface roughness peaks. The probability of such indentations increases with an increase in the number of AFF cycles. Thus, % ΔR_a and % ΔR_{as} increases with an increase in number of AFF cycles (Fig. 17). However, while performing AFF experiments, repeated interaction between the roughness

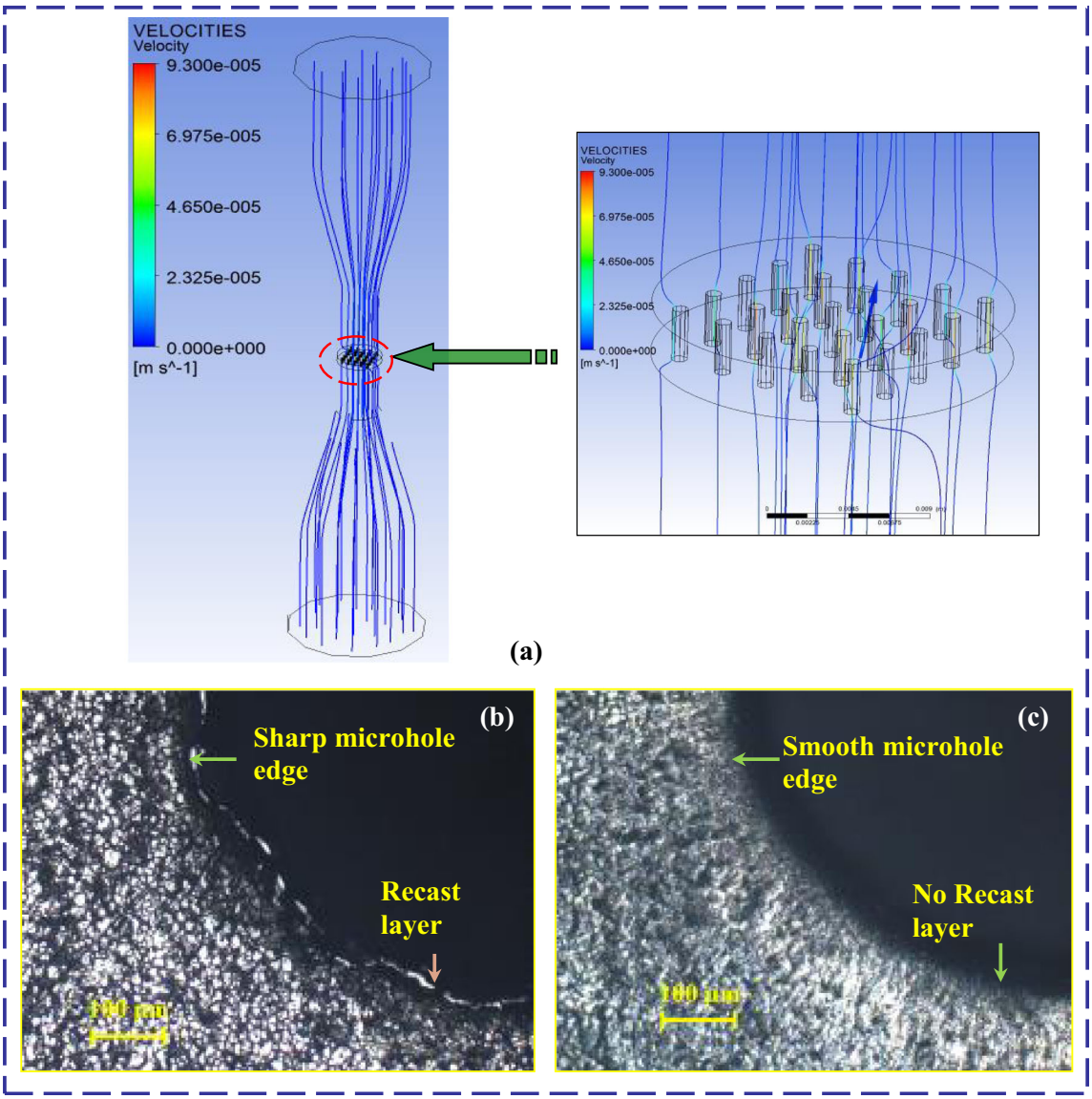

Fig. 20 **a** Velocity streamline of the medium during the AFF process. Microhole edge morphology **b** before finishing and **c** after finishing (8 cycles, # 180, 4 MPa, 53.40 wt.% abrasives particles)

peaks and the abrasive particles leads the bluntness of the sharp cutting edges of the abrasive particles. Thus, abrasive particles lost their capacity to cut the surface roughness peaks effectively and efficiently at the higher number of AFF cycles. As a result, the simulated value of % ΔR_{as} is higher than the experimental % $\Delta R_{a.}$

5.2.3 Effect of wt.% of abrasive particles

Increase in wt.% of the abrasive particles in the medium enhances the performance of the AFF process in two ways. Firstly, as the wt.% of the abrasive particles increases, the magnitude of radial stresses acting on the abrasive particles increases (Fig. 14b). Secondly, the number of abrasive particles per unit time taking part in the cutting action of the surface roughness peaks increases with the increase in wt.% of the abrasive particles in the medium. Thus, an improvement in the surface roughness occurs with the increase in wt.% of the abrasive particles (Fig. 18).

Before finishing operation, microhole surface is very rough due to the presence of re-solidified hard recast layer and loosely bonded metal debris (Fig. 19a). AFF process successfully removes the hard recast layer and provides fine surface roughness on the microhole inner wall (Fig. 19b).

Finishing of microholes with the help of the viscoelastic medium during the AFF process not only removes recast layer from the microhole walls but also provides smooth edges. Viscous component of the medium helps it to flow in the axial direction and the elastic component controls its radial movement.

Due to the elastic nature of the medium after flowing through the restricted microhole passageway at the exit of the microhole, the medium tries to gain its original undeformed shape. As a result, medium moves in radial as well as in axial direction (Fig. 20a). Initial edge of the microhole is irregular with sharp recast micropins formed due to the EDμM process (Fig. 20b). The radial movement of the medium at the microhole exit not only removes debris and recast layer along its inner wall but also provides smoothness on the microhole edges (Fig. 20c). Components made of SS 316L having microholes with finished internal surface and smooth edges (e.g., stents) not only maintains a constant flow rate of fluid carried by them but also prevents its contamination by the addition of loosely bonded metal debris.

Figure 21a shows the 2D surface roughness profile having the initial surface roughness of 1.45 μm. During the experiments after finishing microholes with AFF process, best surface roughness of 130 nm with an improvement of 91.16% in surface roughness is achieved (Fig. 21b). Across the same AFF input parameters, surface roughness of 90 nm with an improvement of 94.14% in surface roughness is predicted during the simulation (Fig. 21c). Thus, there is a reasonable

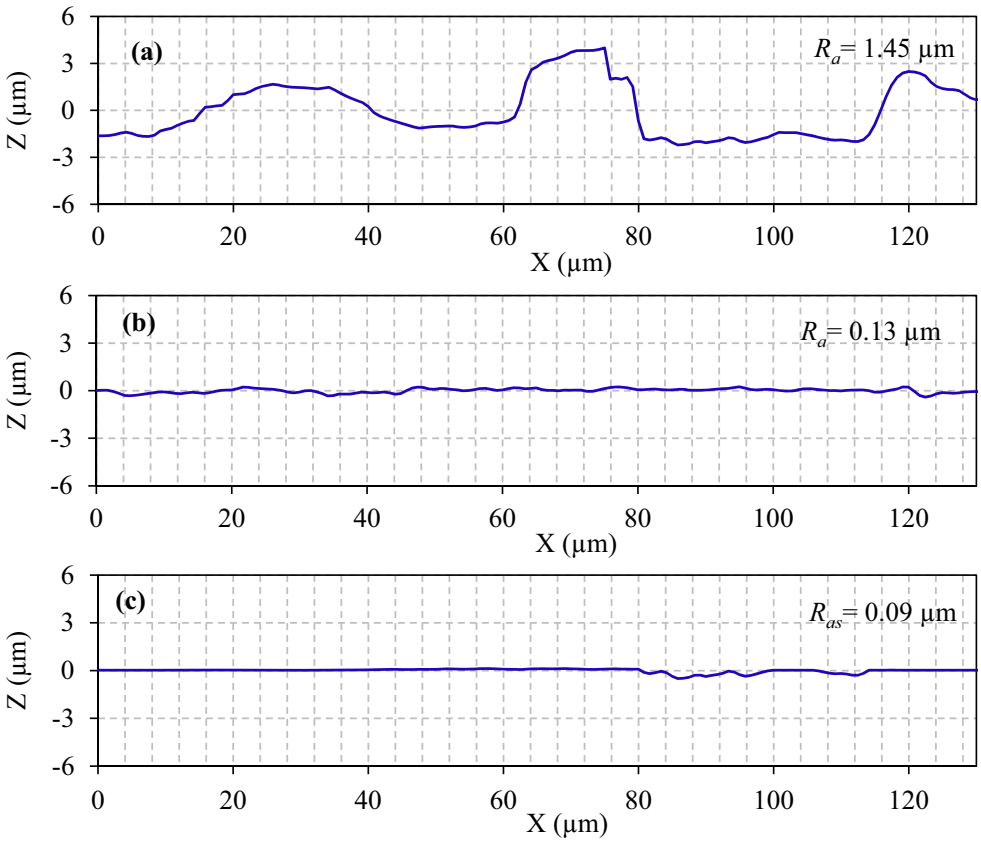

Fig. 21 Two-dimensional surface roughness profile of the microhole surface **a** initial and **b** after performing AFF experiments **c** simulated (8 cycles, # 180, 4 MPa, 53.40 wt.% abrasives particles)

error of 2.96% between the experimental and simulated maximum value of % ΔR.

6 Conclusions

In the present work, FE analysis of the AFF process during the finishing of microholes in surgical stainless steel is carried out. The developed FE model simulates the flow of the viscoelastic medium during the AFF process. Also, a simulation model for predicting surface roughness generated by the AFF process on the workpiece surface is developed. Abrasive particles with multiple cutting edges and the incorporation of the actual initial surface roughness profile during the simulation are few of the many new features of the developed simulation model over the previously developed surface roughness simulation models. Some of the important findings of the current work are

1. 3D FE model of the viscoelastic medium flow during the finishing of microholes by the AFF process is established.
2. Amount of radial stresses generated in the medium increases with the increase in extrusion pressure and wt.% of the abrasive particles.
3. Surface roughness simulation model predicts percentage change in surface roughness with a maximum of 8% error when compared with the experimental results.
4. During the experiments after finishing microholes with AFF process, an improvement of 91.16% in surface roughness is achieved. Across the same AFF input parameters, an improvement of 94.14% in surface roughness is predicted during the simulation.
5. AFF process not only removes hard recast layer from the microhole inner wall but also smoothens its sharp outer edges which are due to the machining process of microholes.
6. Extrusion pressure, number of AFF cycles, and wt.% of the abrasive particles are the important AFF input parameters that determine the final surface roughness of the workpiece surface.

Acknowledgements The authors are thankful for the financial support provided by Board of Research in Nuclear Sciences (Project Number ME/P/MRS/02), Department of Science and Technology for their Technology Systems Development Program (DST/TSG/AMT/2015/619), and Defense Research Development & Development Laboratory (CARS Project).

Nomenclature C, wt.% of the abrasive particles in the medium; D, Rate of deformation tensor; D_{pj}, Diameter of j^{th} abrasive particle; D_{idj}, Indentation diameter of j^{th} abrasive particle; d_j, Maximum indentation depth of j^{th} abrasive particle; f, Internal forces; F_n, F_s, Normal and tangential forces; F_R, Average radial force acting on a single abrasive particle; I, Identity tensor; L_a, Assessment length of the surface roughness profile; L_m, Equivalent length of the medium passed through workpiece in one AFF stroke; L_s, Length of AFF stroke; M_j, Maximum positive difference between the Z coordinates of j^{th} abrasive particle cutting edge and the corresponding Z coordinates of the roughness peak at a particular X coordinate; N_{tmaxj}, Maximum numbers of cutting edges of the j^{th} abrasive particle that can take part in the cutting action of roughness peak; p, Hydrostatic pressure; R_a, Experimental value of surface roughness; R_{as}, Simulated value of surface roughness; R_m, Radius of medium cylinder; R_{pj}, Radius of the j^{th} abrasive particle; r_m, Radius of microhole; T, Total extra stress tensor; $\hat{U}$, Velocity vector; V_n, V_s, Normal and tangential velocities; V_m, Volume of medium; X^0_j, Y^0_j, Z^0_j, Center coordinates of the j^{th} abrasive particle; x_{ir}, X coordinate of the i^{th} roughness peak; x_{iaj}, X coordinate of the i^{th} cutting edge of j^{th} abrasive particle; z_{ir}, Z coordinate of the i^{th} roughness peak; z_{iaj}, Z coordinate of the i^{th} cutting edge of j^{th} abrasive particle; z_m, Maximum height of the roughness peak at a particular AFF stroke; % ΔR_a, Percentage change in experimental value surface roughness; % ΔR_{as}, Percentage change in simulated value surface roughness; α, Material constant; λ, Relaxation time; τ, Extra stress tensor; ρ_a, Density of the abrasive particles; ρ_m, Density of the medium; σ_s, Purely viscous component of extra stress tensor; σ_p, Purely viscoelastic component of extra stress tensor; σ_p^{∇} , Upper-convected derivative of viscoelastic extra stress tensor; η_1, Viscosity factor for the viscoelastic component of the extra stress tensor; η_2, Viscosity factor for purely viscous component of the extra stress tensor; σ_R , Average radial stress generated in the medium

Abbreviations AFF, Abrasive flow finishing; SS, Stainless steel; FE, Finite element; CFD, Computation fluid dynamics; 2D, Two-dimensional; 3D , Three-dimensional; BHN, Brinell hardness number; EDμM, Electrical discharge micro machining; CCRD, Central composite rotatable design

References

1. Loveless TR, Williams RE, Rajurkar KP (1994) A study of the effects of abrasive-flow finishing on various machined surfaces. J Mater Process Technol 47(1–2):133–151
2. Raju HP, Narayanasamy K, Srinivasa YG, Krishnamurthy R (2005) Characteristics of extrude honed SG iron internal primitives. J Mater Process Technol 166(3):455–464
3. Sushil M, Vinod K, Harmesh K (2015) Experimental investigation and optimization of process parameters of Al/SiC MMCs finished by abrasive flow machining. Mater Manuf Process 30(7):902–911
4. Wu MY, Gao H (2016) Experimental study on large size bearing ring raceways' precision polishing with abrasive flowing machine (AFM) method. Int J Adv Manuf Technol 83(9–12):1927–1935
5. Fu Y, Wang X, Gao H, Wei H, Li S (2016) Blade surface uniformity of blisk finished by abrasive flow machining. Int J Adv Manuf Technol 84(5–8):1725–1735
6. Walia RS, Shan HS, Kumar P (2009) Enhancing AFM process productivity through improved fixturing. Int J Adv Manuf Technol 44(7–8):700–709
7. Jain RK, Jain VK, Dixit PM (1999) Modeling of material removal and surface roughness in abrasive flow machining process. Int J Mach Tools Manuf 39(12):1903–1923
8. Jain RK, Jain VK (2003) Finite element simulation of abrasive flow machining. Proc Inst Mech Eng B J Eng Manuf 217(12):1723–1736
9. Jain RK, Jain VK (1999) Simulation of surface generated in abrasive flow machining process. Robot Comput Integr Manuf 15(5):403–412
10. Gorana VK, Jain VK, Lal GK (2006) Prediction of surface roughness during abrasive flow machining. Int J Adv Manuf Technol 31(3–4):258–267

11. Fang L, Sun K, Cen Q (2007) Particle movement patterns and their prediction in abrasive flow machining. Lubr Sci 13(4):195–206
12. Wang AC, Lung TS, Liang KZ, Chun-Ho LI, Shi-Hong WE (2009) Uniform surface polished method of complex holes in abrasive flow machining. Trans Nonferrous Metals Soc China 19:250–257
13. Wan S, Ang YJ, Sato T, Lim GC (2014) Process modeling and CFD simulation of two-way abrasive flow machining. Int J Adv Manuf Technol 71(5–8):1077–1086
14. Dash R, Maity K (2015) Simulation of abrasive flow machining process for 2D and 3D mixture models. Front Mech Eng 10(4): 424–432
15. Chen KY, Cheng KC (2014) A study of helical passageways applied to polygon holes in abrasive flow machining. Int J Adv Manuf Technol 74(5–8):781–790
16. Wang AC, Cheng KC, Chen KY, Lin YC (2014) Enhancing the surface precision for the helical passageways in abrasive flow machining. Mater Manuf Process 29(2):153–159
17. Singh S, Raj AA, Sankar MR, Jain VK (2016) Finishing force analysis and simulation of nanosurface roughness in abrasive flow finishing process using medium rheological properties. Int J Adv Manuf Technol 85(9):2163–2178
18. Petri KL, Billo RE, Bidanda B (1998) A neural network process model for abrasive flow machining operations. J Manuf Syst 17(1): 52–64
19. Mollah AA, Pratihar DK (2008) Modeling of TIG welding and abrasive flow machining processes using radial basis function networks. Int J Adv Manuf Technol 37(9):937–952
20. Hull JB, Fletcher AJ, Trengove SA, Mackie J (1992) Rheology of carrier media used in abrasive flow machining. Key Eng Mater 72: 617–626
21. Davies PJ, Fletcher AJ (1995) The assessment of the rheological characteristics of various polyborosiloxane/grit mixtures as utilized in the abrasive flow machining process. Proc Inst Mech Eng C J Mech Eng Sci 209(6):409–418
22. Fletcher AJ, Fioravanti A (1996) Polishing and honing processes: an investigation of the thermal properties of mixtures of polyborosiloxane and silicon carbide abrasive. Proc Inst Mech Eng C J Mech Eng Sci 210(3):255–265
23. Sankar MR, Jain VK, Ramkumar J, Joshi YM (2011) Rheological characterization of styrene-butadiene based medium and its finishing performance using rotational abrasive flow finishing process. Int J Mach Tools Manuf 51(12):947–957
24. Kar KK, Ravikumar NL, Tailor PB, Ramkumar J, Sathiyamoorthy D (2009) Performance evaluation and rheological characterization of newly developed butyl rubber based media for abrasive flow machining process. J Mater Process Technol 209(4):2212–2221
25. Kar KK, Ravikumar NL, Tailor PB, Ramkumar J, Sathiyamoorthy D (2009) Preferential media for abrasive flow machining. J Manuf Sci Eng 131(1):1–11
26. Uhlmann E, Doits M, Schmiedel C (2013) Development of a material model for visco-elastic abrasive medium in abrasive flow machining. Proc CIRP 8:351–356
27. Uhlmann E, Schmiedel C, Wendler J (2015) CFD simulation of the abrasive flow machining process. Proc CIRP 31:209–214
28. Sankar MR, Ramkumar J, Jain VK (2009) Experimental investigation and mechanism of material removal in nano finishing of MMCs using abrasive flow finishing (AFF) process. Wear 266(7): 688–698

Publisher's Note